COBEM 2021 26th International Congress of Mechanical Engineering
November 22-26, 2021, Virtual Congress, Brazil

COB-2021-1377
GAS-SOLID FLUIDIZED BEDS IN NARROW TUBES

Karlo Fernandes Rocha[a,b,1]
Fernando David Cúñez Benalcázar[a,2]
Erick de Moraes Franklin[a,3]
[a]University of Campinas, School of Mechanical Engineering, Rua Mendeleyev, 200, Campinas, 13083-860, Brazil
[b]Federal Institute of Espírito Santo, Rodovia BR-482 (Cachoeiro-Alegre), 29300-970, Cachoeiro de Itapemirim, ES, Brazil
[1]karlor@ifes.edu.br, [2]fernandodcb@fem.unicamp.br, [3]franklin@fem.unicamp.br

Abstract. *Fluidized beds are extensively used in chemical, pharmaceutical, and mineral industries. For instance, they can be found in a wide range of applications such as coal burning, coal gasification, organic synthesis, mineral processing, and incineration of waste due to their ability to transfer high mass and energy quantities. Over the last years, the increasing use of biomass materials in industrial applications has revived our interest in using fluidized beds. In the case of gas-solid fluidized beds in narrow tubes, instabilities usually appear in the form of granular plugs and bubbles characterized by regions of high and low concentration of particles, respectively. These patterns emerge due to the high confinement effects that come from the low ratio between the sizes of the tube and particles (D/d<10). In this study, the behavior of gas-solid fluidized beds in narrow tubes is investigated numerically. The beds were formed in a vertical tube with an internal diameter of D = 3 mm and were filled with glass spheres with a diameter of d = 0.5 mm. We used two arrangements of beds consisting of 400 and 600 glass beads. Then we imposed three airflow rates at the inlet of the tube that correspond to cross-sectional mean velocities of U = 1.4Umf, U = 1.8Umf, and U = 2Umf, where Umf is the minimum fluidization velocity. Under these conditions, we observed the formation of granular plugs and bubbles that propagate with characteristic lengths and celerities. The numerical simulations were performed using an Eulerian-Lagrangian approach (CFD-DEM), where we used the open-source codes CFDEM, OpenFOAM, and LIGGGHTS. From our results, we tracked every single particle and the local volume fraction of each bed over time to obtain the primary behavior of this problem. Also, we computed and then analyzed the evolution of the granular temperature and the collisions of the particles. Our results bring new contributions on the role of gas-solid fluidized beds in narrow tubes.*

Keywords: *fluidized bed, gas-solid, plugs, CFD-DEM, Eulerian-Lagrangian method*

1. INTRODUCTION

Fluidized beds are extensively used in the chemical, pharmaceutical and mineral industries. They can be found in a wide range of applications such as coal burning, coal gasification, organic synthesis, mineral processing and incineration of waste. In the case of gas-solid fluidized beds, when the velocity of the fluid flow is increased to a certain value, the drag force exerted by the fluid balances with the weight of the particles, reaching thus the suspension of particles. This velocity is known as settling velocity at the inception of fluidization or minimum velocity of fluidization. At higher flow rates the bed may become unstable and part of the fluid passes through the bed in the form of bubbles or slugs. Bubbles occur in beds where the diameter of the tube is large when compared to grain diameters, and are characterized by regions of voids that propagate upwards along the bed, whereas plugs and bubbles occur in narrow diameter beds and are characterized by compact regions of high and low concentration of particles, respectively. This behavior can also occur in narrow solid-liquid fluidized beds (SLFB).

Gas-solid fluidized beds in wide channels and tubes are very unstable and rapidly reach a bubbling regime. Several studies investigated the instabilities appearing in gas fluidized beds (Tsuji *et al.*, 1992; Hoomans *et al.*, 1996; Zhou *et al.*, 2010; Goldschmidt *et al.*, 2002; Xu *et al.*, 2007; Wu *et al.*, 2013; Kafui *et al.*, 2002), however, no one studied the narrow case, where the ratio between the tube and the particles is $D/d < 10$.

Many studies have investigated the instabilities in the gas-solid system using an Eulerian-Eulerian numerical approach. In these simulations, the fluid and solid phases are considered as a continuous media and both can be solved by computational fluid dynamics (CFD), (Cammarata *et al.*, 2003; Mahinpey *et al.*, 2007; Hosseini *et al.*, 2009). Other studies in the literature have used an Eulerian-Lagrangian approach for the study of fluidized beds (Tsuji *et al.*, 1992; Hoomans *et al.*, 1996; Zhou *et al.*, 2010; Goldschmidt *et al.*, 2002) where the solid phase is considered as discrete and the fluid phase is considered as continuous. The solid phase, based on Discrete Element Method (DEM, citepcundall1979discrete), is solved by Newtion's second law of motion applied to a discrete system, while the fluid phase, based on (CFD), is solved by Navier Stokes equations. This approach is also known as CFD-DEM. In the last years, several studies (Tsuji *et al.*, 1992;

Hoomans *et al.*, 1996; Zhou *et al.*, 2010) have demonstrated that CFD-DEM simulations can predict the hydrodynamics of fluidized beds well.

In the case of liquid fluidized beds, they are less unstable than gas fluidized beds and usually present a voidage-wave instability (Anderson and Jackson, 1969; Zenit and Hunt, 2000; Duru and Guazzelli, 2002; Aguilar-Corona *et al.*, 2011; Ghatage *et al.*, 2014). For the very narrow case, Cúñez and Franklin (2019), studied experimentally and numerically the behavior of liquid fluidized beds, where the ratio between the tube and particle diameters was $D/d = 4.23$. The beds were formed in a tube with an internal diameter of $D = 25.4$ mm and consisted of alumina particles with a diameter of $d = 6$ mm. With these conditions, the authors observed the formation of the granular plugs and piston bubbles. They also found that the characteristic lenghts of the plugs for this specific case were around 7 to 9 particle diameters.

In this work, we present CFD-DEM computations to investigate the confinement effects in gas-solid fluidized beds of circular cross section. Depending on the ratio between the tube and particle diameters, such effects lead to the formation of alternating high- and low-compactness regions, known as plugs and piston bubbles, which have characteristic lengths and velocities. The gas-solid fluidized beds were formed in a 5 cm long vertical tube with a diameter of $D = 3$ mm and were filled with glass spheres with a diameter of $d = 0.5$ mm and density of $\rho_p = 2500$ kg/m^3. Thus, the ratio between the tube and the particles was $D/d = 6$. We computed the characteristic lengths and celerities of the plugs, the trajectories of individual grains, and also investigate numerically the granular temperature in the plug and bubble regions. We report the particle granular temperature based on the spatial averaging of squared fluctuation velocity of particles.

2. FORMULATION OF THE NUMERICAL MODEL

The mass and momentum equations for the gas phase are given respectively by

$$\frac{\partial \rho_f \varepsilon_f}{\partial t} + \nabla \cdot (\rho_f \varepsilon_f \vec{u}_f) = 0 \tag{1}$$

$$\frac{\partial \rho_f \varepsilon_f \vec{u}_f}{\partial t} + \nabla \cdot (\rho_f \varepsilon_f \vec{u}_f \vec{u}_f) = -\varepsilon_f \nabla P + \varepsilon_f \nabla \cdot \vec{\bar{\tau}} + \rho_f \varepsilon_f \vec{g} + \vec{F}_{p,f} \tag{2}$$

where P represent the pressure, $\vec{g}$ is the acceleration of gravity, $\vec{\bar{\tau}}$ is the deviatoric stress tensor and $\rho_f, \varepsilon_f, \vec{u_f}$ are the density, volume fraction and mean velocity of the fluid, respectively. The last term $\vec{F}_{p,f}$ on the right represents the drag force per volume, being computed by Gidaspow model (Gidaspow, 1994) and given by

$$\vec{F}_{p,f} = \frac{1}{V_{cell}} \sum \vec{F}_d = \frac{1}{V_{cell}} \sum \frac{V_{p_i} \beta}{(1-\varepsilon_f)} (\vec{u}_f - \vec{u}_p) \tag{3}$$

where β is the coefficient of momentum transfer between phases due to the drag force, V_{cell} is the volume of each cell and V_{p_i} is the volume of particle i in cell. The coefficient β is given by

$$\beta = \begin{cases} 150 \dfrac{(1-\varepsilon_f)^2 \mu_f}{\varepsilon_f d_p^2} + 1.75 \dfrac{\rho_f |\vec{u}_f - \vec{u}_p| (1-\varepsilon_f)}{d_p}, & \varepsilon_f < 0.8 \\ \dfrac{3}{4} C_d \dfrac{\rho_f \varepsilon_f (1-\varepsilon_f) |\vec{u}_f - \vec{u}_p|}{d_p} \varepsilon_f^{-2.65}, & \varepsilon_f \geq 0.8 \end{cases} \tag{4}$$

where C_d is the drag coefficient and is related to the particle Reynolds number by

$$C_d = \begin{cases} \dfrac{24}{Re_p} \left(1 + 0.15 \left(Re_p\right)^{0.687}\right), & Re_p < 1000 \\ 0.44, & Re_p \geq 1000 \end{cases} \tag{5}$$

with

$$Re_p = \frac{\rho_f \varepsilon_f d_p |\vec{u}_f - \vec{u}_p|}{\mu_f}. \tag{6}$$

For the solid phase, the motion of each particle is calculated by linear and angular momentum equations and are given by

$$m_p \frac{d\vec{u}_p}{dt} = -V_p \nabla P + V_p \nabla \cdot \vec{\bar{\tau}} + m_p \vec{g} + \left[\sum_{i,j} \vec{F}_{c,i,j} + \sum_{i,w} \vec{F}_{c,i,w} \right] - \vec{F}_{p,f} \tag{7}$$

$$I_p \frac{d\vec{\omega}}{dt} = \sum_{i,j} \vec{T}_{p,i,j} + \sum_{i,w} \vec{T}_{p,i,w} \tag{8}$$

where $\vec{u_p}$, m_p, V_p are the velocity, mass and volume of the solid particle, respectively. T_p is the torque from the tangential component of the contact force, and I_p and $\vec{\omega}$ are the moment of inertia and angular velocity of a particle, respectively.

For particle-particle interactions, the spring-dashpot model is employed for the contact force $\vec{F}_{c,i,j} = \vec{F}_{cn,i,j} + \vec{F}_{ct,i,j}$ where $\vec{F}_{cn,i,j}$ and $\vec{F}_{ct,i,j}$ are normal and tangential components. The main equations of the spring-dashpot model are described in Cundall and Strack (1979).

2.1 Numerical setup

In the numerical simulations, we considered a gas-solid fluidized bed in a 5 cm long vertical tube with a diameter of $D = 3$ mm and filled with glass spheres with a diameter of $d = 0.5$ mm, and the fluid was air. Two different beds were arranged, consisting of 400 and 600 glass beads, and three air flows corresponding to cross-sectional mean velocities of $\overline{U} = 1.4U_{mf}$, $\overline{U} = 1.8U_{mf}$ and $\overline{U} = 2U_{mf}$ m/s were imposed at the tube inlet, where U_{mf} is the minimum fluidization velocity. Initially, the particles are randomly inserted to fall freely without air flow until they reach the bottom of the tube. After a certain time the bed reaches a stable state with velocity of the particles equal to zero. Thereafter, the fluid flow is initiated at the inlet. The side walls of the tube are impenetrable and with no-sliping conditions for the fluid. The superficial velocity $\overline{U}$ is imposed as the velocity of the air in the vertical direction at the bottom of the tube, where the velocity gradient of the fluid is zero.

This numerical computations are based on Eulerian-Lagrangian method. The fluid flow is solved based CFD with the open source code OpenFOAM (www.openfoam.com), the granular motion is solved with the open source code LIGGGHTS (www.liggghts.com) which is based on DEM, and CFD-DEM coupling is made with the open source code CFDEM (www.cfdem.com). A three dimensional geometry of vertical tube was created and generated a hexahedral mesh with a total number of 38.400 cells. We employed a big particle void fraction model (www.cfdem.com), which is used when the particle is larger than the CFD cells. With the generated mesh, the behavior of the grains inside the fluid flow was well captured. For CFD-DEM simulations, the fluctuations of the particles and the particle-particle interactions are stronger than the velocity fluctuations of the fluid-flow. In addition, for the fluid phase, the Reynolds number is of the order 200 so we have a laminar regime. Therefore, the mesh refinement is unnecessary. We run the numerical simulations over 5 seconds for all the cases. For that, each run took approximately 18 to 20 hours to be completed. Finally, all the simulations were performed using a configuration hardware Intel Core i9-9900K 3.60GHz with 8 core and 64 GB RAM.

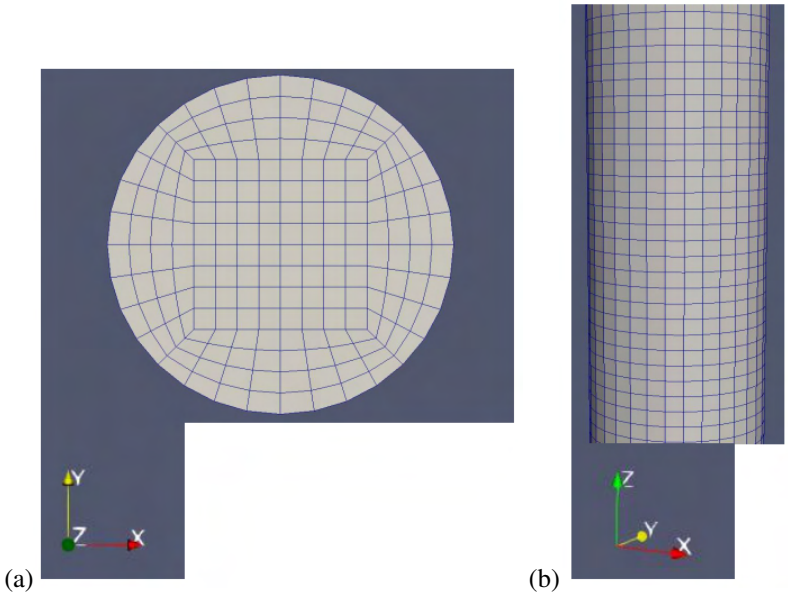

(a) (b)

Figure 1. Hexahedral mesh with a total number of 38.400 cells.

The parameters used in simulations are following: tube diameter $D = 3$ mm; number of particles $N = 400$ and $N = 600$; particle diameter $d = 0.5$ mm; particle density $\rho_p = 2500$ Kg/m^3; gas density $\rho_f = 1.2$ Kg/m^3; gas viscosity $\mu_f = 1.8$ kg.m^{-1}s^{-1}; Young's Modulus $E = 0.6$ GPa; Poisson ratio $\sigma = 0.3$; Restitution coefficient $e = 0.9$ Friction coefficient 0.4; time step for CFD 1×10^{-5} s; time step for DEM 1×10^{-7} s. The corresponding parameters of Young's Modulus, Poisson ratio, Restitution coefficient and Friction coefficient were considered based on the studies Tsuji *et al.* (1992); Hoomans *et al.* (1996); Zhou *et al.* (2010).

3. RESULTS

3.1 Fluidized Bed

In this section, we present the results of the main behavior of gas-solid fluidized beds. The minimum fluidization velocity is given by

$$U_{mf} = \frac{d^2(\rho_p - \rho_f)g}{150\mu_f}\left(\frac{\varepsilon_f^3}{(1-\varepsilon_f)}\right) \tag{9}$$

where g is the acceleration of gravity. With $g = 9.81$ m/s^2 and $\varepsilon_f = 0.51$, we estimate $U_{mf} = 0.6144$ m/s. Numerically, considering the figure of the pressure drop as a function of the superficial velocity, U_{mf} was estimated as 0.633 m/s when the pressure drop stabilizes, as can be seen in the figure 2.

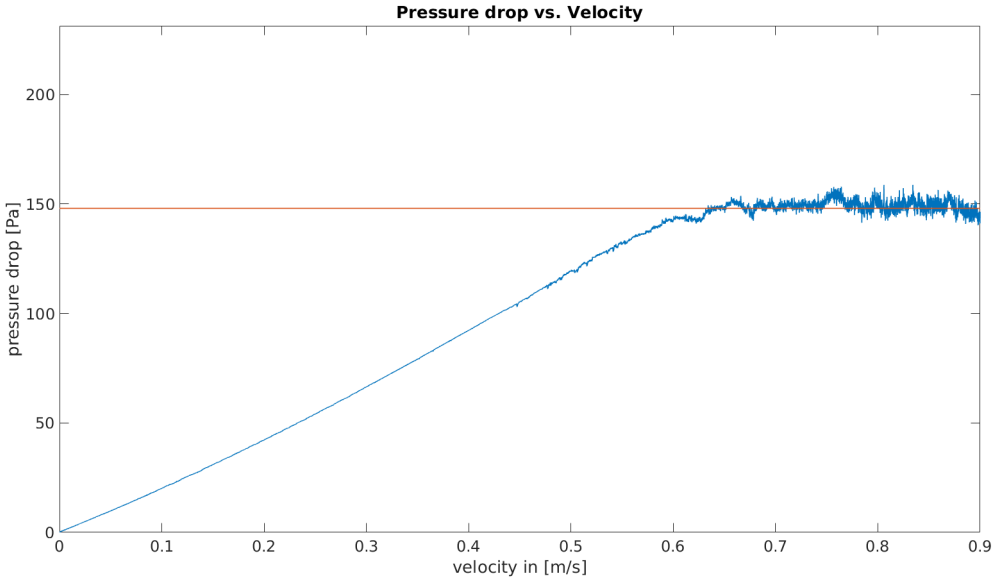

Figure 2. The pressure drop versus velocity

Figure 3 presents instantaneous snapshots of the bed with $N = 600$ particles and for flow rates $\overline{U} = 1.8U_{mf}$ m/s, respectively. The corresponding times are: $t = 0$, $t = 1$,$t = 1.5$, $t = 2$,$t = 2.5$, $t = 3$, $t = 3.5$, $t = 4$ and $t = 4.5$ seconds.

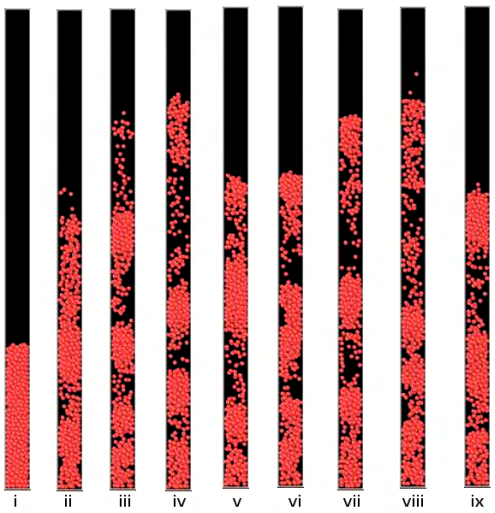

Figure 3. $N = 600$, $\overline{U} = 1.8U_{mf}$ m/s and times i) $t = 0$ s; ii) $t = 1$ s; iii) $t = 1.5$ s; iv) $t = 2$ s; v) $t = 2.5$ s; vi) $t = 3$ s; vii) $t = 3.5$ s; viii) $t = 4$ s; ix) $t = 4.5$ s.

In the simulated conditions, granular plugs and bubbles occupying the entire tube cross section were observed in the

fluidized bed. These patterns presented almost one-dimensional shape, that propagates upwards and downwards with characteristic lengths and velocities. The curve in Fig. 4 represents the solid volume fraction (SVF) of the granular bed inside the tube. Regions of high-compactness of particles, where SVF is greater than 0.5, were considered as plugs. Thus, based on the SVF curve, we have identified and followed the particles in each granular plug and bubble over the 5 seconds of simulation.

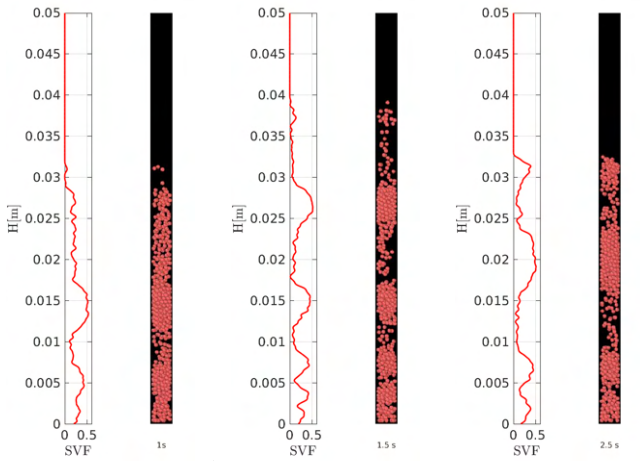

(a) (b) (c)

Figure 4. SVF curve, $N = 600$ and $\overline{U} = 1.8U_{mf}$ m/s, times a) $t = 1$ s; b) $t = 1.5$ s; c) $t = 2.5$ s.

3.2 Granular Plugs

The granular plugs and piston bubbles occupying the entire tube cross section were observed in the fluidized bed. These patterns presented almost one-dimensional shape, that propagated upwards and downwards with characteristic lengths and velocities. We have identified and followed each granular plug using numerical scripts in MATLAB. In this way, it was possible to calculate the characteristic lengths of the plugs λ, the upward V_{up} and downward V_{down} velocities of the top of the bed, and the standard deviation of length scale σ_λ, upward velocity $\sigma_{V,up}$, and downward velocity $\sigma_{V,down}$. These data are presented in Tab. 1.

Table 1. Number of particles N, superficial velocity $\overline{U}$, plug upward velocity of the top of the bed V_{up}, plug downward velocity of the top of the bed V_{down}, length scale of plugs λ, length scale of plugs normalized by the grain diameter λ/d, initial bed height h and average height of the fluidized bed h_m, standard deviation of plug upward velocity $\sigma_{V,up}$, standard deviation of plug downward velocity $\sigma_{V,down}$, standard deviation of length scale σ_λ

Case	a)	b)	c)	d)	e)	f)
N	400	400	400	600	600	600
$\overline{U}$ (m/s)	$1.4U_{mf}$	$1.8U_{mf}$	$2U_{mf}$	$1.4U_{mf}$	$1.8U_{mf}$	$2U_{mf}$
V_{up} (m/s)	0.0294	0.0829	0.1036	0.1219	0.1381	0.1475
V_{down} (m/s)	-0.0694	-0.3942	-0.4781	-0.2961	-0.1936	-0.2529
λ (m)	0.0057	0.0031	0.0024	0.0055	0.003	0.0027
λ/d	11.4	6.2	4.8	11.0	6.0	5.4
$\sigma_{V_{up}}$ (m/s)	0.0153	0.0503	0.0765	0.1175	0.1288	0.1138
$\sigma_{V_{down}}$ (m/s)	0.0282	0.3721	0.416	0.2916	0.165	0.1611
σ_λ (m)	0.003	0.0011	0.0011	0.003	0.0014	0.0014
$\sigma_{\lambda/d}$	6.0	2.2	2.2	6.0	2.8	2.8
h (m)	0.007	0.007	0.007	0.0101	0.0101	0.0101
h_m (m)	0.0098	0.0122	0.0141	0.0131	0.0216	0.0261

In order to show the macroscopic structure of the bed, we placed side by side snapshots of particle positions in simulations, and present them, respectively, in Figs. 5. We note that for lower velocities, close to the minimum fluidization velocity, an upward displacement of most of the bed occurs almost in the form of a single structure, that is, a single granular plug. While at higher speeds, the bed breaks down into smaller plug structures.

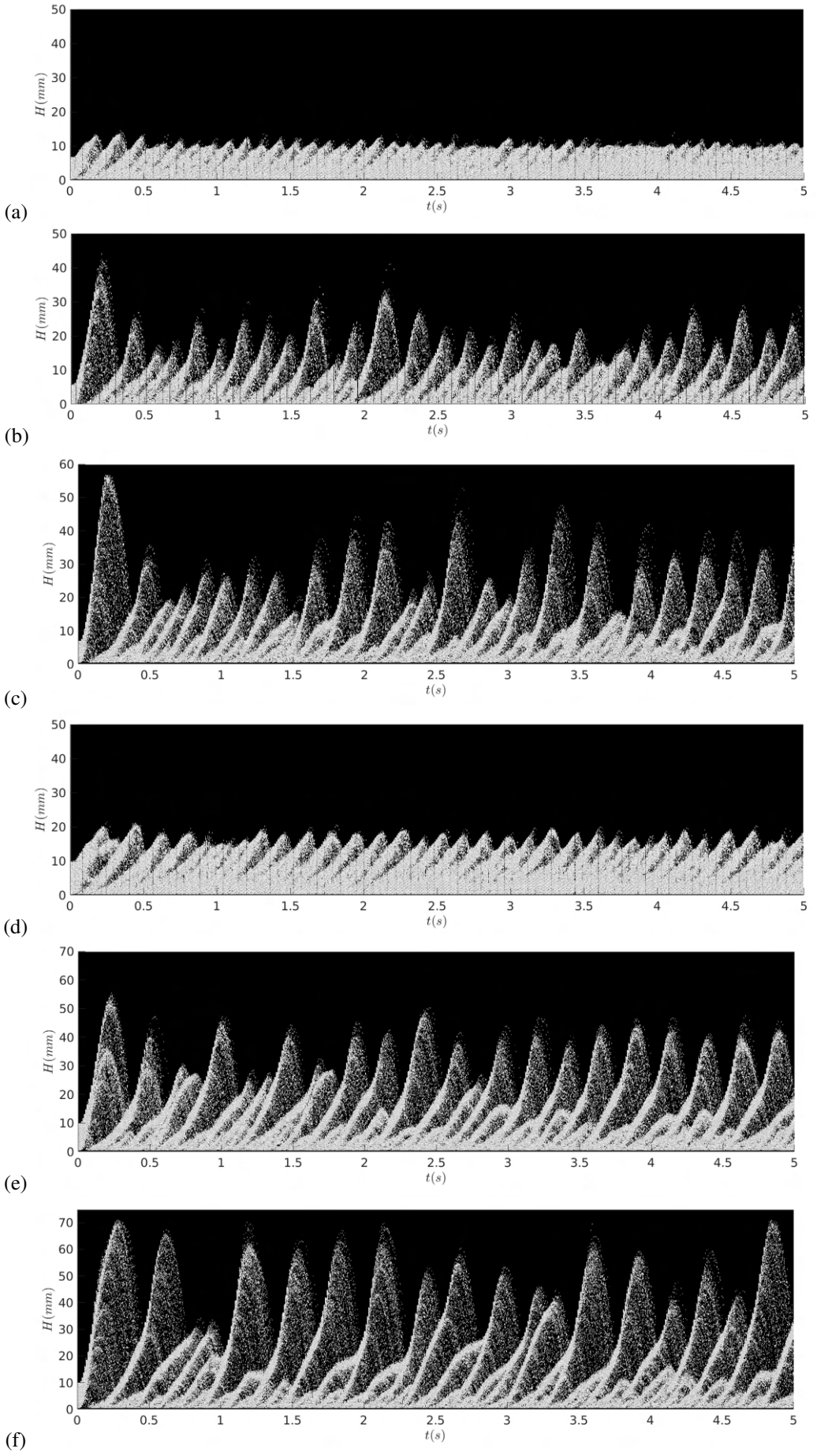

Figure 5. Snapshots of particle positions, from numerical simulations, for beds consisting of 400 and 600 particles, placed side by side. N=400 (a) $\overline{U} = 1.4U_{mf}$; (b) $\overline{U} = 1.8U_{mf}$; (c) $\overline{U} = 2U_{mf}$; N=600 (d) $\overline{U} = 1.4U_{mf}$; (e) $\overline{U} = 1.8U_{mf}$; (f) $\overline{U} = 2U_{mf}$

3.3 Granular Temperature

The fluctuating velocities of the particles are the main point to define the granular temperature in a particulate system. For systems that evolve in time, an apparent granular temperature might be defined based on the fluctuations in the bulk motion as a function of time (Jung *et al.*, 2005). In addition, a granular temperature can be defined based on the velocities fluctuations due to the interaction between the solid phase and the gas phase (Campbell, 2006). In general, in all previous works, these definitions of granular temperature are reasonable, the important point to define the granular temperature of a particle system being to establish the objective of the investigation to be done. For instance, in the kinetic theory of granular flows, it is interesting to understand the relative (translational) motion between particles, in this sense, we consider in this study the definition of granular temperature characterizing these particle fluctuation velocities which is given as follows. The velocity fluctuation is given by the measured instantaneous particle velocity $v(\vec{x}, t)$ minus the mean velocity of particles $\langle v(\vec{x}, t)\rangle$. The mean velocity of is defined as

$$\langle v_k(t)\rangle = \frac{1}{n}\sum_{i=1}^{n} v_k(i,t) \tag{10}$$

where k represents x, y, and z directions and n is the number of particles. Consider the square mean of the velocity fluctuations of each particle as a function of time t is given by:

(a)

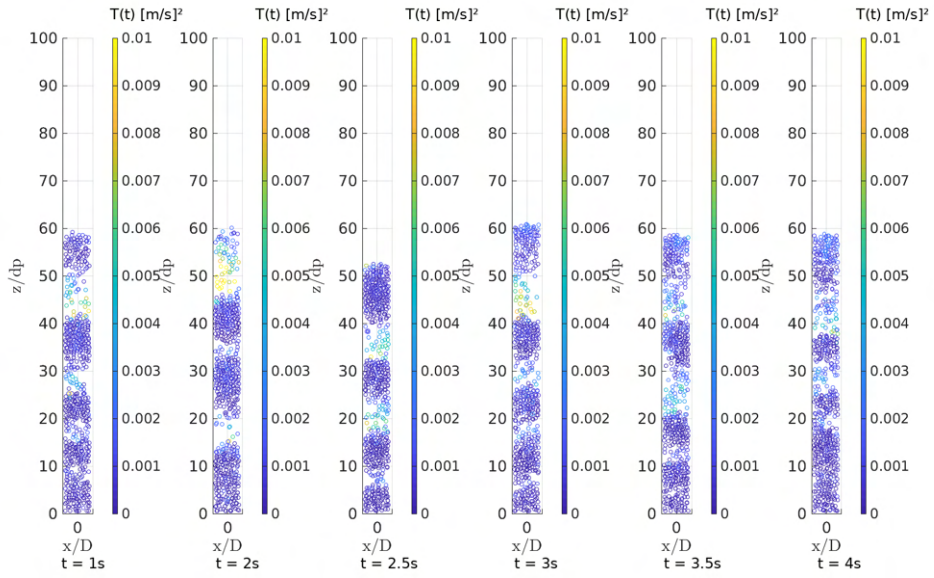

(b)

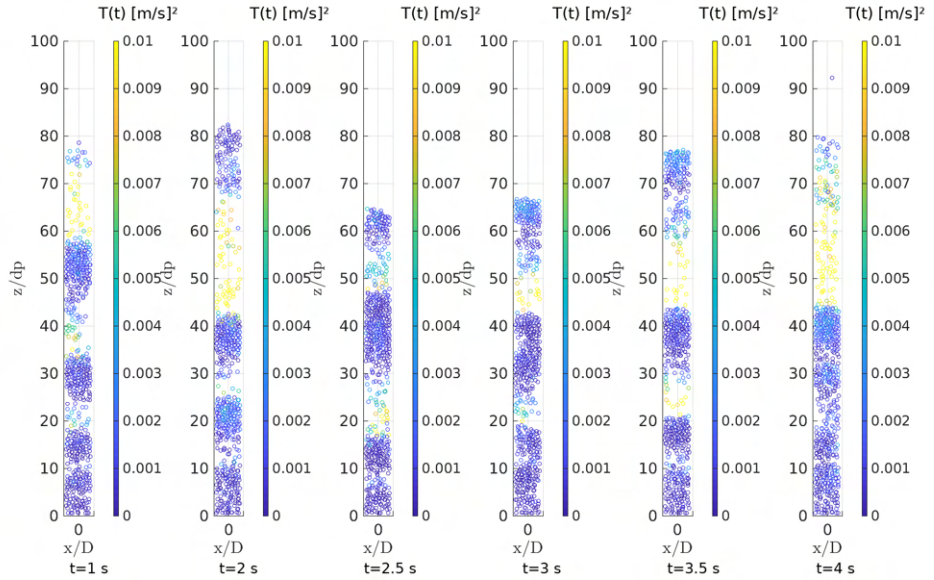

Figure 6. $N = 600$. a) $\overline{U} = 1.4U_{mf}$; b) $\overline{U} = 1.8U_{mf}$

$$T(t) = \frac{T_x(t) + T_y(t) + T_z(t)}{3} \tag{11}$$

where $T_k(t) = [v_k(t) - \langle v_k(t) \rangle]^2$ with $k = x, y, z$. Equation 11 defines the granular temperature of the bed at time t. Figure 6 presents the positions of the center of the particles in the x, z directions and the color bar represents the intensity of $T(t)$, in the corresponding times $t = 1$, $t = 2$,$t = 2.5$, $t = 3$, $t = 3.5$ and $t = 4$ seconds.

Note that, in the Fig. 6, there are regions that show homogeneous fluctuations. In regions of high particle compactness, where SVF is close to 0.5, the square mean of the particles velocities fluctuations is low, and where there is low compactness is high. Plugs have low oscillation of particles, and bubbles high oscillation.

4. CONCLUSIONS

This work investigated numerically a gas-solid fluidized bed in a narrow tube. The confinement effects created by ratio between the tube and grain diameters $D/d = 6$ leads to the formation of alternating high- and low-compactness regions. These regions, known as plugs and piston bubbles, respectively, occupy the entire tube cross section, oscillating upwards and downwards with characteristic lengths and velocities. The granular temperature was computed, in plugs and bubbles, by averaging the instantaneous velocities by using the concepts of kinetic theory.

The numerical simulations were based on Eulerian-Lagrangian method. We performed three dimensional simulations using a CFD-DEM method with the open source code CFDEM. Two different beds were arranged, consisting of $N = 400$ and $N = 600$ glass beads, and air flows corresponding to cross-sectional mean velocities of $\overline{U} = 1.4U_{mf}$, $\overline{U} = 1.8U_{mf}$ and $\overline{U} = 2U_{mf}$ m/s were imposed. We have identified and followed each granular plug in simulations using numerical scripts written in MATLAB, and calculated the characteristic length λ, the upward V_{up} and downward V_{down} velocities of the top of the beds.

The lengths of plugs had variations with the increase of the superficial velocity $\overline{U}$. The velocities V_{up} and V_{down} of the top of the bed presented variations between 0.0294 m/s and 0.1475 m/s and -0.2529 m/s and -0.0694 m/s, respectively.

The granular temperature reaches the highest values in the bubbles because the intensity of particle oscillations is much greater in bubbles than in plugs.

5. ACKNOWLEDGEMENTS

Fernando Cúñez is grateful to FAPESP (Grants no. 2016/18189-0 and 2018/23838-3) and Erick Franklin to FAPESP (Grant No. 2018/14981-7), and to CNPq (Grant No. 400284/2016-2) for the financial support provided. Karlo Rocha is grateful to the IFES-FEM/UNICAMP Dinter.

6. REFERENCES

Aguilar-Corona, A., Zenit, R. and Masbernat, O., 2011. "Collisions in a liquid fluidized bed". *Int. J. Multiphase Flow*, Vol. 37, No. 7, pp. 695 – 705.

Anderson, T.B. and Jackson, R., 1969. "A fluid mechanical description of fluidized beds. Comparison of theory and experiment". *Ind. Eng. Chem. Fundamen.*, Vol. 8, No. 1, pp. 137–144.

Cammarata, L., Lettieri, P., Micale, G. and Colman, D., 2003. "2d and 3d cfd simulations of bubbling fluidized beds using eulerian-eulerian models". *International J. of Chemical Reactor Engineering*.

Campbell, C.S., 2006. "Granular material flows - an overview." *Powder Technol.*, Vol. 162, pp. 208–229.

Cúñez, F.D. and Franklin, E.M., 2019. "Plug regime in water fluidized beds in very narrow tubes". *Powder Technol.*, Vol. 345, pp. 234–246.

Cundall, P.A. and Strack, O.D., 1979. "A discrete numerical model for granular assemblies". *Géotechnique*, Vol. 29, No. 1, pp. 47–65.

Duru, P. and Guazzelli, É., 2002. "Experimental investigation on the secondary instability of liquid-fluidized beds and the formation of bubbles". *J. Fluid Mech.*, Vol. 470, pp. 359–382.

Ghatage, S.V., Peng, Z., Sathe, M.J., Doroodchi, E., Padhiyar, N., Moghtaderi, B., Joshi, J.B. and Evans, G.M., 2014. "Stability analysis in solid-liquid fluidized beds: Experimental and computational". *Chem. Eng. J.*, Vol. 256, pp. 169 – 186.

Gidaspow, D., 1994. *Multiphase flow and fluidization: continuum and kinetic theory descriptions*. Academic press.

Goldschmidt, M.V., Beetstra, R. and Kuipers, J.M., 2002. "Hydrodynamic modelling of dense gas-fluidised beds: Comparison of the kinetic theory of granular flow with 3d hard-sphere discrete particle simulations". *Chemical Engineerin Science*, Vol. 57, pp. 2059–2075.

Hoomans, P.B., Kuipers, M., A., Brierls, W.J. and Van Swaaij, P.M., 1996. "Discrete particle simulation of bubble and slug formation in a two dimensional gas-fluidised bed: a hard-sphere approach". *Chemical Engineerin Science*, Vol. 51, No. 1, pp. 99–118.

Hosseini, S.H., Rahimi, R., Zivdar, M. and Samimi, A., 2009. "Cfd simulation of gas-solid bubbling fluidized bed

containing fcc particles." *Korean J. Chem. Eng.*, Vol. 26(5), pp. 1405–1413.

Jung, J., Gidaspow, D. and Gamwo, I.K., 2005. "Measurement of two kinds of granular temperatures, stresses, and dispersion in bubbling beds." *Industrial and Engineering Chemistry Research.*, Vol. 44, pp. 1329–1341.

Kafui, K.D., Thornton, C. and Adams, M.J., 2002. "Discrete particle-continuum fluid modelling of gas-solid fuidised beds". *Chemical Engineerin Science*, Vol. 57, pp. 2395–2410.

Mahinpey, N., Vejahati, F. and Ellis, N., 2007. "Cfd simulation of gas-solid bubbling fluidized bed: an extensive assessment of drag models." *WIT Transactions on Engineering Sciences*, Vol. 56, pp. 51–60.

Tsuji, Y., Tanaka, T. and Ishida, T., 1992. "Lagrangian numerical simulation of plug flow of cohesionless particles in a horizontal pipe". *Powder Technol.*, Vol. 71, No. 3, pp. 239–250.

Wu, G., Ouyang, J. and Li, Q., 2013. "Revised drag calculation method for coarse grid lagrangian-eulerian simulation of gasâĂŞsolid bubblingfluidized bed". *Powder Technol.*, Vol. 235, pp. 959–967.

Xu, M., Ge, W. and Li, J., 2007. "A discrete particle model for particle-fluid flow with considerations of sub-grid structures". *Chemical Engineerin Science*, Vol. 62, pp. 2302–2308.

Zenit, R. and Hunt, M.L., 2000. "Solid fraction fluctuations in solid-liquid flows". *Int. J. Multiphase Flow*, Vol. 26, No. 5, pp. 763 – 781.

Zhou, Z.Y., Kuang, S.B., Chu, K.W. and Yu, A.B., 2010. "Discrete particle simulation of particle fluid flow: model formulations and their applicability". *J. Fluid Mech.*, Vol. 661, pp. 482–510.